Reducing scalloping in synthetic aperture radar images using a composite image transform

Knut Landmark, Anne H. Schistad Solberg

Knut Landmark, Anne H. Schistad Solberg, "Reducing scalloping in synthetic aperture radar images using a composite image transform," Proc. SPIE 9643, Image and Signal Processing for Remote Sensing XXI, 96431B (15 October 2015); doi: 10.1117/12.2194952

SPIE.

Event: SPIE Remote Sensing, 2015, Toulouse, France

Reducing scalloping in synthetic aperture radar images using a composite image transform

Knut Landmark[a] and Anne H. Schistad Solberg[b]

[a]Norwegian Defence Research Establishment, PO Box 25, NO-2027 Kjeller, Norway;
[b]Department of Informatics, PO Box 1080, NO-0316 Oslo, Norway

ABSTRACT

In burst mode SAR imaging, echo intensity depends on the target's azimuth position in the antenna pattern. As a result, an amplitude modulation known as scalloping may appear, particularly in ScanSAR images of ocean areas. A denoising method, recently developed for multibeam bathymetry, can be used to reduce residual scalloping in ScanSAR images. The algorithm is analogous to a band-stop filter in the frequency domain. Here, the transform is the composition of an edge detection operator and a discrete Radon transform (DRT). The edge operator accentuates fine-scale intensity changes; the DRT focuses linear features, as each DRT component is the sum of pixel intensities along a linear graph. A descalloping filter is implemented in the DRT domain by suppressing the range direction. The restored image is obtained by applying the inverse composite transform. First, a rapidly converging iterative pseudo-inverse DRT is computed. The edge operator is a spatial filter based on a discrete approximation of the Laplace operator, but modified to make the operator invertible. The method was tested on ocean scene ScanSAR images from the Envisat Advanced Synthetic Aperture Radar. The scalloping effect was significantly reduced, with no apparent distortion or smoothing of physical features.

Keywords: Discrete Radon transforms, edge detection operators, image restoration, iterative methods, Laplace operator, scalloping, ScanSAR, stripe noise, synthetic aperture radar

1. INTRODUCTION

In burst mode synthetic aperture radar (SAR) imaging, a point target is illuminated for only a part of the time it lies within the radar beam footprint. Consequently, the received echo intensity depends on the azimuth (along-track) antenna pattern and the target's azimuth angles relative to the beam centre, during the burst. This azimuth dependence may cause artifacts in SAR imagery, including azimuth scalloping, a periodic modulation of the image intensity in the azimuth direction[1] (Fig. 1). SAR image formation includes beam pattern and descalloping corrections. In particular, if several adjacent looks overlap, weighting functions may be applied when summing the contributions of each look to reduce the azimuth dependence.[2] However, this requires accurate estimates of the beam centre or Doppler centroid, otherwise a residual scalloping remains. Residual scalloping has been seen, in particular, in wide-swath ScanSAR images of ocean areas, and may interfere with image recognition tasks such as surface wind or wave field mapping[3] and oil spill detection.[4]

Corrections for scalloping may also be implemented as a postprocessing step applied to SAR image products. For example, a descalloping filter can be implemented using wavelet transforms, as demonstrated by Schiavulli et al.[5] Ripel[4] achieved good results by scaling pixel intensities with a row-dependent correction factor. The original image, and a smoothed version without scalloping, were summed along the horizontal (column) dimension to obtain two row vectors whose element-wise ratio yielded the correction factors. The analysis of Romeiser et al[3] highlights the complexity of the scalloping modulation. They too obtain the final image by multiplying the noisy image with an array of correction factors, i.e., scalloping is treated as multiplicative noise. The correction factors are obtained by spectral peak analysis and masking in the frequency (Fourier transform) domain, with iterative refinement to eliminate secondary artifacts introduced by spectral

Further author information: (Send correspondence to K.L.)
K.L.: E-mail: knut.landmark@ffi.no, Telephone: +47 6380 7683
A.H.S.S.: E-mail: anne@ifi.uio.no, Telephone: +47 2285 2435

Image and Signal Processing for Remote Sensing XXI, edited by Lorenzo Bruzzone, Proc. of SPIE
Vol. 9643, 96431B · © 2015 SPIE · CCC code: 0277-786X/15/$18 · doi: 10.1117/12.2194952

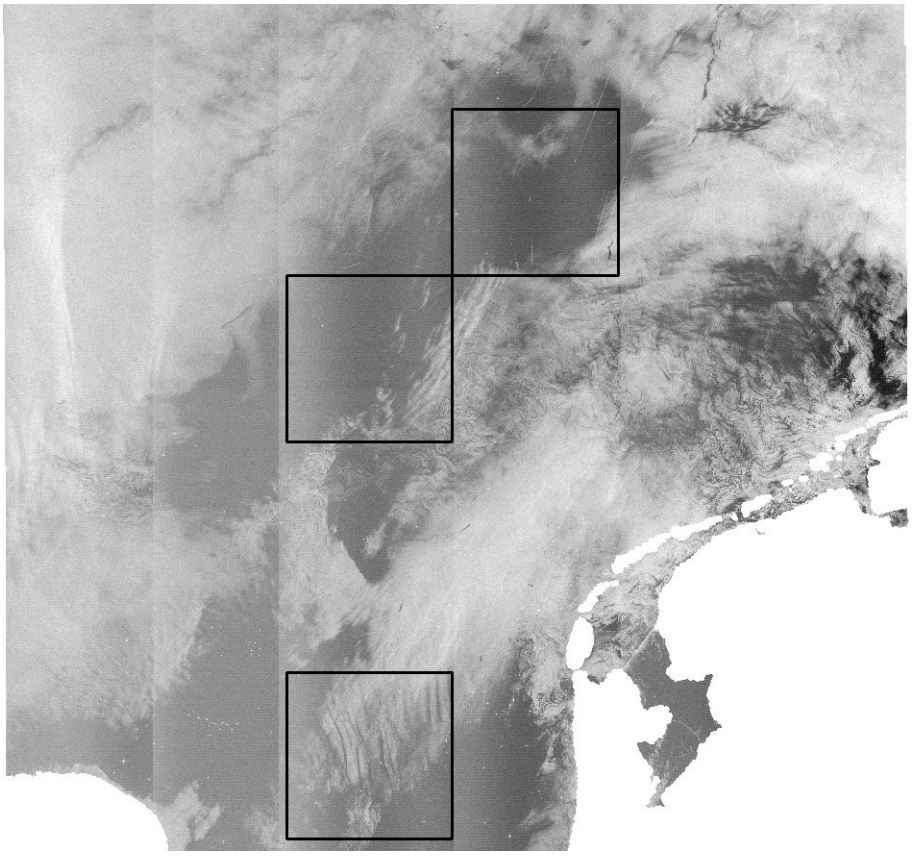

Figure 1. ENVISAT ASAR ScanSAR image (wide swath mode) of the southern North Sea, with landmask applied. (To the lower right, the Dutch coast roughly from the Hague and northwards; to the lower left, a part of Norfolk, England.) The contrast of the image has been adjusted to make it appear less dark in print. Scalloping, an amplitude modulation in azimuth direction, is seen as faint, densely spaced horizontal stripes. The effect of the denoising algorithm is demonstrated on three subimages with 1024×1024 pixels, marked by the black frames (Sec. 3) ©ESA/KSAT.

peak suppression. In general, any descalloping filter, whether transform based or implemented in the spatial domain, should remove artifacts with as little smoothing or distortion of physical features as possible.

A new image restoration method was recently developed for reducing track line artifacts and motion-induced errors in multibeam echo sounder bathymetry.[6] We demonstrate that the method, with minor modifications, can be successfully applied to remove residual scalloping in processed ScanSAR images. The method is system independent and analogous to an image filter in the Fourier or wavelet transform domains, with no assumptions about noise periodicity or orientation. In Sec. 2, the main points of this algorithm are reviewed. The algorithm was applied to ocean scene images from the Envisat Advanced Synthetic Aperture Radar (ASAR). In Sec. 3, the effect is demonstrated using three 1024×1024 pixels frames taken from the SAR image in Fig. 1. The paper concludes, in Sec. 4, with a short discussion on results, limitations, and possible improvements.

2. ALGORITHM

The proposed denoising method has three elements: an edge detection operator $\mathcal{L}$, a discrete Radon transform (DRT) $\mathcal{R}$, and an approximation operator $\mathcal{T}$. The algorithm is analogous to applying a band-stop filter in the Fourier transform (frequency) domain. Here, the transform is the composite operator $\mathcal{R} \circ \mathcal{L}$. The operator $\mathcal{L}$ accentuates fine-scale intensity changes, and $\mathcal{R}$ focuses linear features because each DRT component is the sum of pixel intensities along a linear graph. For an image $f \in \mathbb{R}^{N \times N}$, the DRT, $r = \mathcal{R}[f]$, may be represented by a matrix where each element $r_{i,j}$ corresponds to a particular slope and intercept, and the

column index j uniquely identifies the slope, i.e., orientation (Sec. 2.2). The filter is implemented by zeroing the elements of r in a narrow band of columns given by the orientation of the noise. For azimuthal scalloping, this means the direction perpendicular to the satellite track.

The composite operator $\mathcal{R} \circ \mathcal{L}$ is applied to the detrended image $f - \mathcal{T}[f]$, where $\mathcal{T}[f] \sim f$ is an approximation that does not preserve noise or artifacts (Sec. 2.3). If this step is omitted, large values of $\mathcal{L}[f]$ along the boundary of the image may be altered by the DRT domain filter, causing distortions in the restored image. Finally, the inverse operator $(\mathcal{R} \circ \mathcal{L})^{-1} = \mathcal{L}^{-1} \circ \mathcal{R}^{-1}$ is applied and the trend $\mathcal{T}[f]$ added back to obtain the restored image. Note that, the filtered DRT r' (with "band-stop" filter applied) is in general not in the range of $\mathcal{R}$. Consequently, the inverse DRT, $\mathcal{R}^{-1}$, acts as a pseudo-inverse operator (Sec. 2.2). The complete procedure is summarized as Algorithm 1. The following subsections provide brief reviews of the basic elements of the algorithm. A more detailed analysis may be found in Ref. 6.

Algorithm 1 Reduce scalloping

Precondition: $f \in \mathbb{R}^{N \times N}$ is a square image of size $N \times N$ pixels, where N is a power of 2
Require: Index, c, of DRT column corresponding to range direction
Require: Half-width, w (number of DRT columns), of band-stop filter

```
function DESCALLOPING(f)
    t ← T[f]
    r ← R[L(f − t)]
    for j ← c − w to c + w do
        for all rows i do                    ▷
            r_{i,j} ← 0
    f ← L^{-1}[R^{-1}(r)]
    return f + t
```

2.1 Edge operator

The Laplace operator (or Laplacian) in Euclidean space $\mathbb{R}^d$ is linear, rotation invariant, edge sensitive, and noise sensitive. It is defined by $\Delta f = \nabla \cdot \nabla f$, for $f : \mathbb{R}^d \to \mathbb{R}$ twice differentiable, and related to neighborhood averages by[7]

$$\lim_{r \to 0} \frac{1}{r^2 \operatorname{Vol}\left(B^d(x;r)\right)} \int_{B^d(x;r)} [f(y) - f(x)] \, \mathrm{d}^{\mathrm{d}}y = \frac{1}{2(d+2)} \Delta f(x), \tag{1}$$

where $\operatorname{Vol}\left(B^d(x;r)\right)$ is the volume of the d-dimensional ball $\{\, y \in \mathbb{R}^d : \|y - x\| < r \,\}$. Equation (1) shows that Δ accentuates boundaries between distinct regions such that the the local value $\Delta f(\boldsymbol{x})$ is independent of the orientation of the structures it detects. For $d = 2$, a discrete approximation to the Laplacian is obtained by convolution with the point spread function (PSF)

$$h = \frac{1}{2} \begin{bmatrix} 1/2 & 1 & 1/2 \\ 1 & -6 & 1 \\ 1/2 & 1 & 1/2 \end{bmatrix}. \tag{2}$$

The transfer function of this PSF, zero-padded to size $N \times N$ elements, is[8]

$$\mathcal{F}[h]_{mn} = 4\left[\cos^2(k_x/2)\cos^2(k_y/2) - 1\right] \approx -k^2 + \frac{3}{32}k^4 - \frac{1}{96}\cos(4\phi)k^4 + \mathcal{O}(k^6) \tag{3}$$

where the scaled wave number $\boldsymbol{k} = 2\pi \begin{bmatrix} m & n \end{bmatrix} / N$, for $m, n = 0, \ldots, N-1$, is expressed in polar coordinates k, ϕ. This operator is isotropic for small wave numbers.

Both Eqn. (3) and the continuous transfer function, $\Delta(\boldsymbol{k}) \sim -k^2$, vanish for $k = 0$. Let h_M^0 denote the matrix obtained by symmetrically zero-padding Eqn. (2) to size $M \times M$, and let $\eta_M(\epsilon)$ be an $M \times M$ matrix

where the elements η_{mn} are random numbers such that $|\eta_{mn}| \leq \epsilon \ll 1$. A modified Laplacian PSF is obtained by

$$\hat{h} = h_M^0 + \eta_M(\epsilon). \tag{4}$$

The edge operator $\mathcal{L}$ is defined as

$$\mathcal{L}[f] = f * \hat{h} \tag{5}$$

where $*$ denotes circular convolution. Except for improbable (and replaceable) choices for $\eta_M(\epsilon)$, the PSF $\mathcal{F}[\hat{h}]$ does not have zeros, and the inverse is obtained by direct deconvolution, i.e.,

$$\mathcal{L}^{-1}[g] = \mathcal{F}^{-1}\left[\mathcal{F}[g] ./ \mathcal{F}[\hat{h}]\right] \tag{6}$$

where ./ denotes element-wise division. It is understood that $\mathcal{F}[\hat{h}]$ has the same dimension as $\mathcal{F}[f]$, obtained after zero-padding $\hat{h}$ and circularly shifting the DFT. Furthermore,

$$\lim_{\epsilon \to 0} \mathcal{F}[\hat{h}] = \mathcal{F}[h]. \tag{7}$$

Provided $\epsilon \ll 1$, the operator $\mathcal{L}$ therefore has the same desirable properties as the standard discrete Laplacian.

2.2 Discrete Radon transform

The Radon transform of a function $f : \mathbb{R}^n \to \mathbb{R}$ integrates f over hyperplanes in $\mathbb{R}^n$, in particular, straight lines in $\mathbb{R}^2$.[9] In Refs. 10 and 11, a discrete approximation to the 2D Radon transform was presented, in which the line integrals are replaced by sums of pixel intensities along certain graphs that include exactly one pixel from each column in the zero-padded image (matrix). The algorithm is recursive, with $4N^2 \log_2 N$ arithmetic operations (additions) for $N \times N$ pixels images. This is faster than conventional $\mathcal{O}(N^3)$ algorithms. Specifically, let $f_{i,j} \in \mathbb{R}^{N \times N}$ denote the pixel intensity in row i and column j, where $f_{i,j} = 0$ for i, j outside the range $0 \leq i, j < N - 1$, and the lower left corner pixel is $(0, 0)$. The image size N must be a power of 2. In the first quadrant, i.e., for slopes from $0°$ to $45°$, a graph representing a straight line starts at pixel $(h, 0)$ and ends at $(h + s, N - 1)$, where h is the intercept and s is the slope; this graph is denoted $D_N(h, s)$. The same notation may be applied to the subgraphs obtained when the image is recursively split in vertical halves to produce subimages of size $N \times N/2$, $N \times N/4$, $\ldots, N \times 1$. Graphs in subimages of size $N \times 1$ contain a single pixel. The full graph is constructed recursively by combining subgraphs in pairs of adjacent subimages, according to the rule[10–12]

$$D_n(h, 2s) = D_{n/2}^{(L)}(h, s) \cup D_{n/2}^{(R)}(h + s, s) \tag{8a}$$

$$D_n(h, 2s + 1) = D_{n/2}^{(L)}(h, s) \cup D_{n/2}^{(R)}(h + s + 1, s). \tag{8b}$$

Here, the right-hand side of the union refers to the right (R) half of the image, and correspondingly for the left-hand (L) side. The procedure is illustrated in Fig. 2. Slopes in the other quadrants are obtained by transposing or flipping the image. The full DRT is the disjoint union of four parts (quadrants):

$$(\mathcal{R}^1 f)(h, s) = \sum_{(i,j) \in D_N(h,s)} f_{i,j} \qquad (0° \text{ to } 45°) \tag{9a}$$

$$(\mathcal{R}^2 f)(h, s) = \sum_{(i,j) \in D_N(h,s)} f_{j,i} \qquad (45° \text{ to } 90°) \tag{9b}$$

$$(\mathcal{R}^3 f)(h, s) = \sum_{(i,j) \in D_N(h,s)} f_{j,N-1-i} \qquad (-90° \text{ to } -45°) \tag{9c}$$

$$(\mathcal{R}^4 f)(h, s) = \sum_{(i,j) \in D_N(h,s)} f_{N-1-i,j} \qquad (-45° \text{ to } 0°). \tag{9d}$$

The number of non-zero elements in each quadrant is at most $N^2 + N(N - 1)/2$, and the minimum value for h is $-N + 1$, for which the associated graph intersects the image only at a corner pixel. The range $\mathcal{R}\left[\mathbb{R}^{N \times N}\right]$

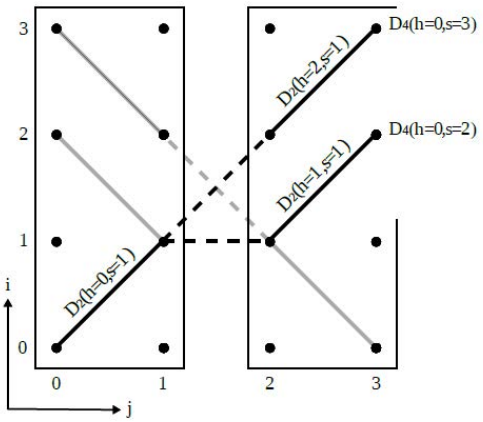

Figure 2. Recursive construction of graphs in a 4×4 pixels image. The graphs are formed by joining graphs in the two 4×2 pixels subimages according to the rule in Eqn. (8). The rise parameter s ranges from 0 to 1 in 4×2 subimages, and from 0 to 3 in the 4×4 image. When the image is flipped upside down, the graphs are mapped to lines with slopes in the range $-45°$ to $0°$ (faint lines). (Illustration from Ref. 6.)

therefore has dimension $P = 4(N^2 + N(N-1)/2) = 6N^2 - 2N$, and $\mathcal{R} : \mathbb{R}^Q \to \mathbb{R}^P$ is a linear operator between vector spaces, with $Q = N^2$.

There is also a recursive, linear adjoint algorithm, $\mathcal{R}^+ : \mathbb{R}^P \to \mathbb{R}^Q$,[11] whose matrix representation is the transpose of the matrix representation of $\mathcal{R}$.[6] If $g = \mathcal{R}^+ \mathcal{R}[f]$, then $g_{i,j}$ is the sum of f along all graphs containing pixel (i,j), i.e., g is the backprojection of $\mathcal{R}[f]$. Press[12] has devised an approximate inverse algorithm for $\mathcal{R}$, here denoted $\mathcal{B}$, which is based on the adjoint operator $\mathcal{R}^+$. Suppose $r' \in \mathbb{R}^P$ is obtained by applying the "band-stop" filter to $r = \mathcal{R}[f]$ (Algorithm 1). We define a pseudo-inverse, $\mathcal{R}^{-1}[r']$, as the solution of the linear system

$$\mathcal{B}\mathcal{R}f = \mathcal{B}r'. \tag{10}$$

This solution is found iteratively by applying the Krylov method GMRES (Generalized Minimum Residual).[13] Writing $b = \mathcal{B}r'$ and $\mathcal{A} = \mathcal{B}\mathcal{R}$, GMRES solves the set of least squares problems

$$x_k = \min_{x \in \mathcal{K}_k(\mathcal{A},b)} \|b - \mathcal{A}x\|, \; k = 1, 2, \ldots \tag{11}$$

where $\mathcal{K}_{k+1}(\mathcal{A}, b) \equiv \text{span}\{ b, \mathcal{A}b, \ldots, \mathcal{A}^k b \}$ is a Krylov subspace. In linear algebra terms, this algorithm involves only matrix-vector multiplications that are implemented by the recursive algorithms $\mathcal{B}$ and $\mathcal{R}$. As a stopping criterion, either a set number of iterations, k (Eqn. 11), or a threshold on the residual $\epsilon = \|b - \mathcal{A}x_k\| / \|b\|$ may be used.

2.3 Approximation

The image $f \in \mathbb{R}^{N \times N}$ is downsampled to size $N/D \times N/D$, and interpolated back to size $N \times N$ using a Chebyshev polynomial tensor product basis of total degree p. The approximation algorithm, $\mathcal{T}$, therefore has two adjustable parameters, D and p. In practice, these are the only parameters that may need tuning in the descalloping method (Algorithm 1). Here, both N and D are taken to be powers of two, with $1 \leq D < N$. Interpolation is accomplished via the expansion

$$f(x,y) \approx \sum_{0 \leq j+k \leq p} w_{jk} T_j(x) T_k(y), \tag{12}$$

where $\{ T_k(x) \}_{k=0}^{\infty}$ is the set of Chebyshev polynomials of the first kind on the interval $[-1,1]$, and the image f is regarded as a set of evenly spaced discrete samples on the square $[-1,1] \times [-1,1]$. There are

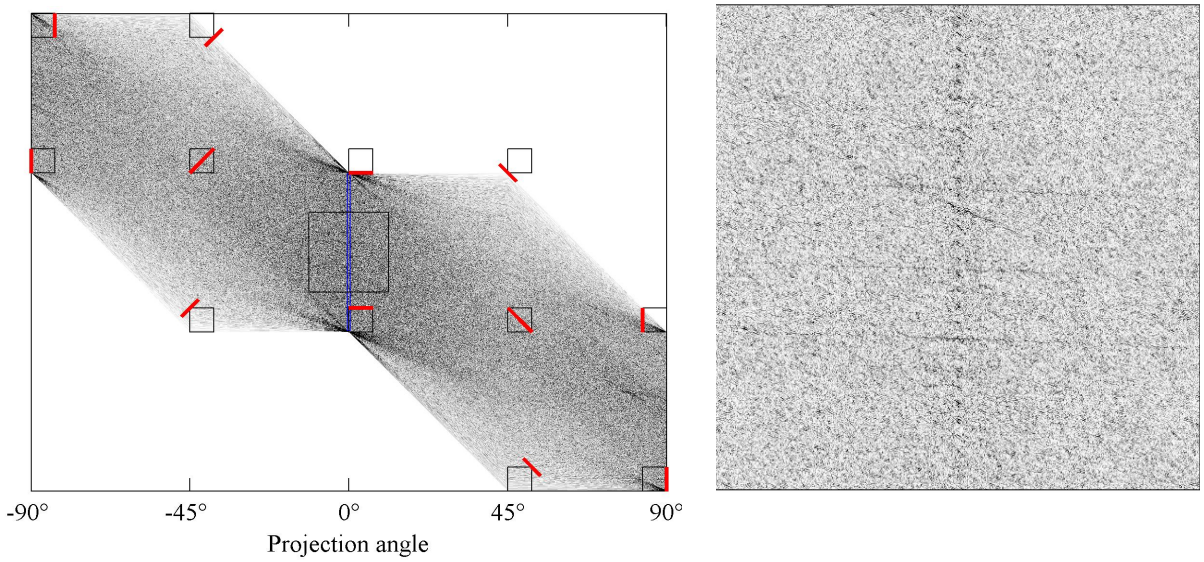

(a) DRT (all quadrants) (b) Close-up

Figure 3. The transform $(\mathcal{R} \circ \mathcal{L})(f - \mathcal{T}[f])$, where f is the 1024×1024 pixels image in Fig. 4a. The four quadrant transforms (Eqn. 9) fit together in a Möbius band.[12] The color map is symmetric about zero, so that white corresponds to zero and black corresponds to high positive or negative values. The close-up in (b) [black rectangle in (a)] shows the signature of scalloping at 0° projection angle. For selected pixels in the DRT, the red lines in (a) indicate which projection the pixel corresponds to, with the small squares symbolizing the image frame. For example, the topmost non-zero value at 0° is the sum along the bottom horizontal line in the SAR image.

$\eta_p = \sum_{d=0}^{p} \binom{d+1}{d} = (p+2)(p+1)/2$ terms in Eqn. (12). As long as N and p are not too large, the coefficients w_{jk} may be determined by multiplication of the down-sampled image with a generalized matrix inverse of size $\eta_p \times (N/D)^2$, which may be computed in advance.[6]

3. EXAMPLES

The method was tested on Envisat ASAR images of ocean areas. The images were aquired in wide swath (WS) mode, where the instrument switches between five adjacent antenna beams. The polarization is VV, and the incidence angle range is 17°–42°. Each image covers approximately 400×400 km, with a range/azimuth resolution of 150×150 m; the range and azimuth pixel spacing is 75 m. The data were originally processed by Kongsberg Satellite Services (KSAT) (Tromsø, Norway), for the purpose of oil spill detection (see, e.g., Refs. 14 and 15). The examples shown below are 1024×1024 pixels subimages of the full image in Fig. 1, taken over the southern North Sea. This image has two visible artifacts. The first is a residual azimuthal scalloping, appearing as faint, periodical, horizontal stripes. The second artifact is a gain shift between adjacent beams, which produces the vertically oriented discontinuities. Scalloping modulations in adjacent beams (subswaths) are not in phase. Therefore, the descalloping algorithm is most effective when applied to each beam separately. We have not attempted to correct the gain shift artifact.

Figure 3a shows the composite transform of the subimage in Fig 4a. Each column has a fixed rise parameter, s, corresponding to a fixed projection angle; the angle is positive clockwise, with 0° along the horizontal (positive x) axis. The DRT is the union of the four quadrant transforms, $\mathcal{R}^1, \ldots, \mathcal{R}^4$ (Eqn. 9), which have been translated vertically so that they fit together in a Möbius band.[12] A unit (one row) increase along the vertical axis corresponds to a unit change in the intercept parameter h, but each row has constant h only within each quadrant separately. A close-up (Fig. 3b) shows a string of points at 0° projection angle, with slightly increased intensity; this is the effect of scalloping. The band-stop filter is implemented by zeroing all pixel values in the blue rectangle in Fig. 3a. The width of the rectangle is approximately 0.6° (15 pixels).

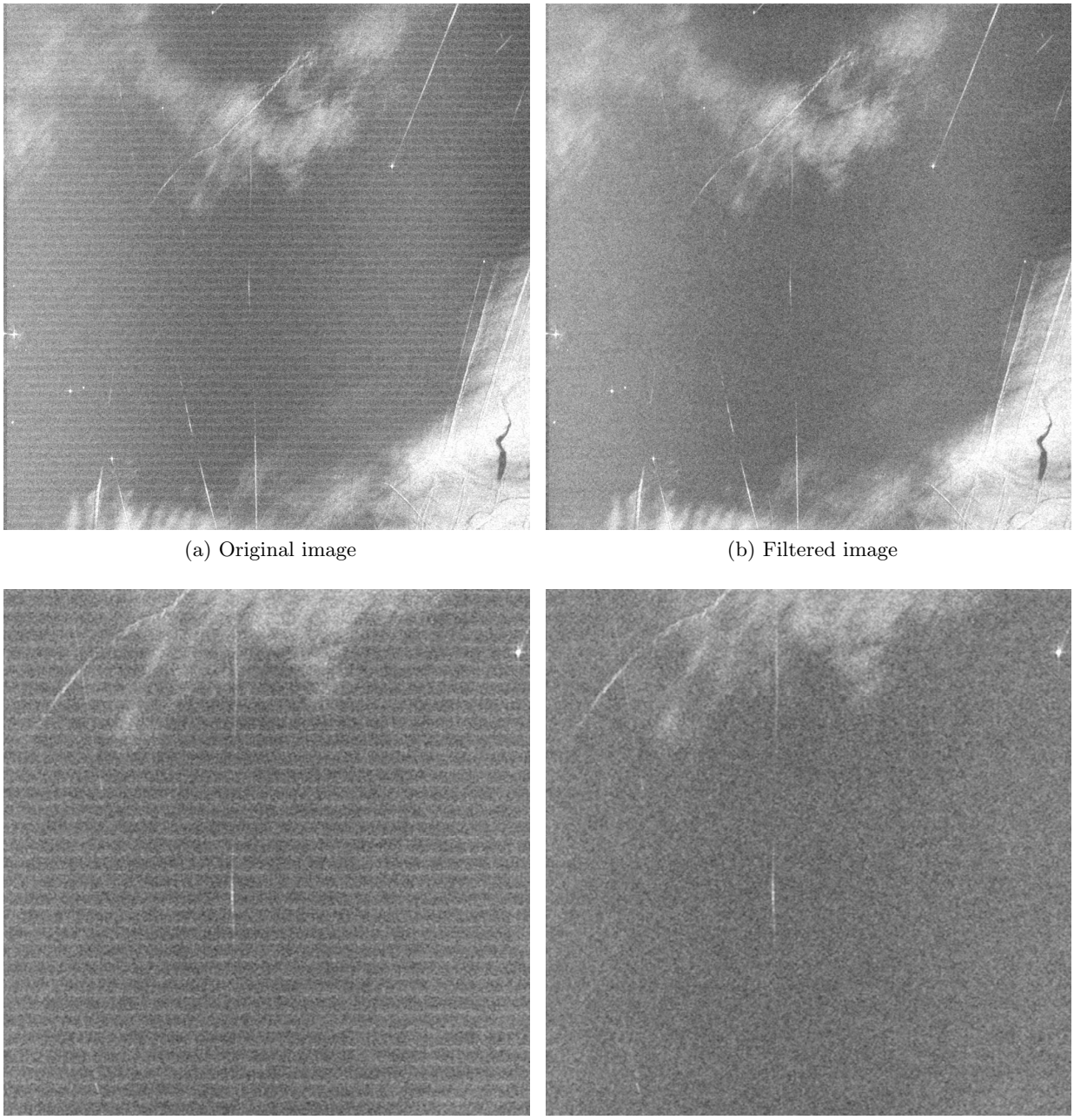

(a) Original image (b) Filtered image

(c) Original image ($2\times$ zoom) (d) Filtered image ($2\times$ zoom)

Figure 4. Effect of the descalloping filter applied to a 1024×1024 pixels subimage (top frame in Fig. 1) ©ESA/KSAT.

The effect of the descalloping filter is shown in Figs. 4–6. The contrast has been increased to make the images look less dark in print and to better show the scalloping. The scaling is identical for all images. These results were obtained with the parameters $p = 18$ and $D = 8$ for the approximation operator $\mathcal{T}$ (Sec. 2.3), and $M = 7$ and $\epsilon = 10^{-3}$ for the edge operator $\mathcal{L}$ (Sec. 2.1). The maximum number of iterations with the GMRES algorithm was six, but two to three iterations also produced satisfactory results. A slight residual scalloping may still be discerned in the upper parts of Figs. 4b and 6b. However, the scalloping effect is seen to be significantly reduced in the filtered images, and there is no apparent distortion or smoothing of physical features.

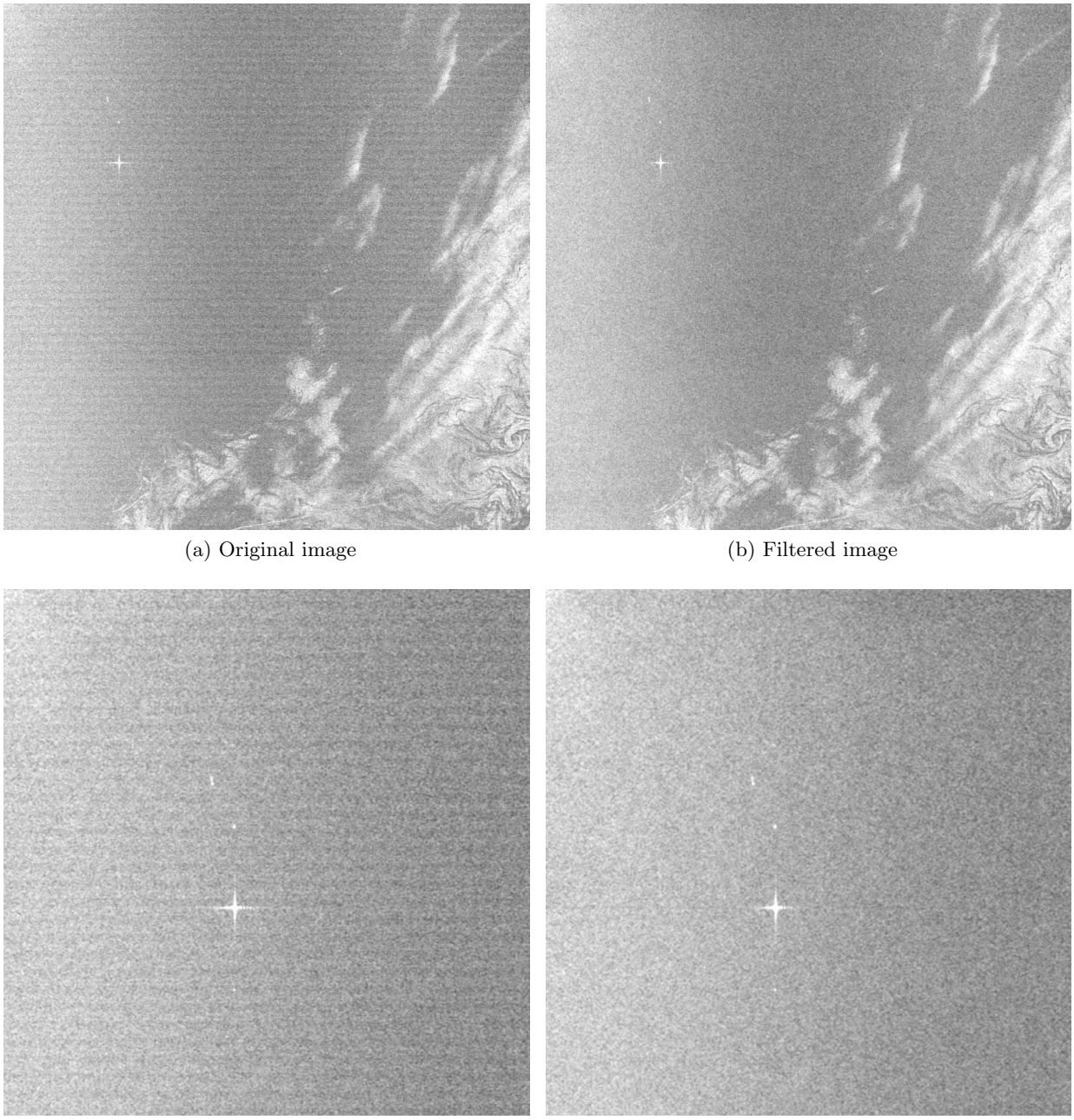

(a) Original image (b) Filtered image

(c) Original image (2 × zoom) (d) Filtered image (2 × zoom)

Figure 5. Effect of the descalloping filter applied to a 1024 × 1024 pixels subimage (middle frame in Fig. 1). ©ESA/KSAT

4. DISCUSSION

Slightly better results are expected with a more careful filter design, e.g., by minimizing the width of the "band-stop" filter or by replacing the peaks and troughs at 0° projection angle with neighborhood values. The restored images in Figs. 4–6 were obtained directly, without experimentation and parameter tuning. While this is encouraging, the aforementioned possibility of incurring low-frequency distortions with the wrong approximation, $\mathcal{T}[f]$, is still a concern (see Sec. 2). This effect can be amended by altering the parameters p and D (see Sec. 2.3), but we feel a more automatic, fail-safe method should be implemented

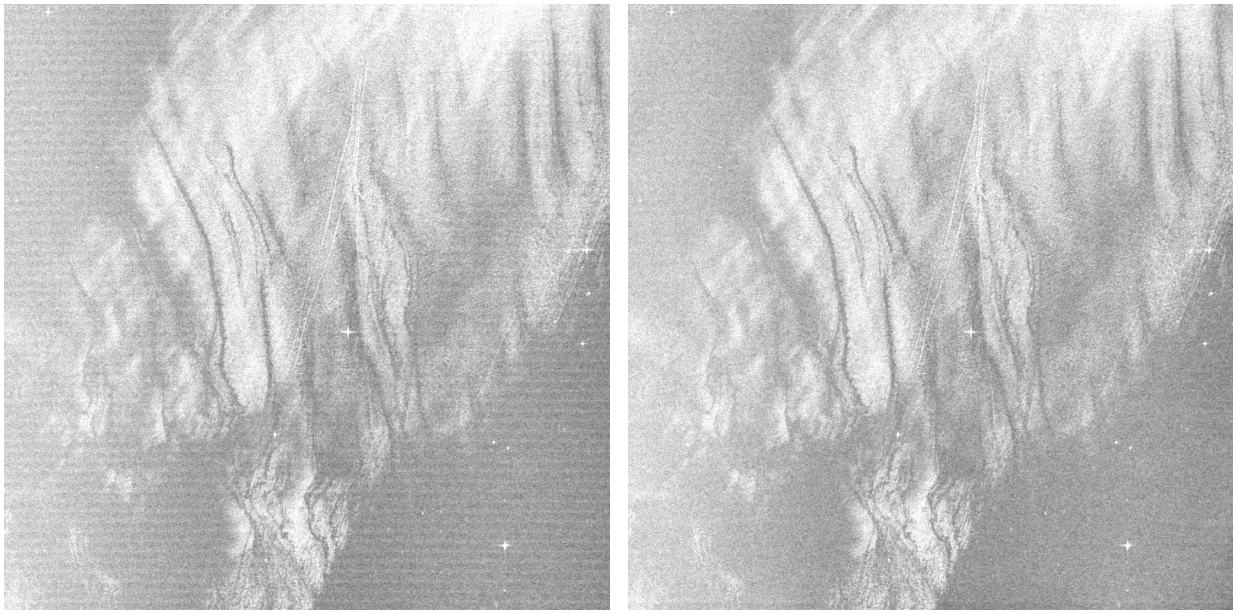

(a) Original image (b) Filtered image

Figure 6. Effect of the descalloping filter applied to a 1024×1024 pixels subimage (lower frame in Fig. 1). ©ESA/KSAT

if the algorithm were to be used in large-scale data processing. The approximation operator was developed for multibeam bathymetry, with track-line artifacts that are preserved to a high degree by standard low-pass filters.[6] Scalloping has quite different characteristics, and low-pass filters are more effective in this instance. It may therefore be that a simple averaging filter can replace the polynomial approximation operator in this particular application.

The DRT[10,11] implemented here is a fast algorithm that does not involve interpolation between pixels. It yields directly a formulation of the inverse problem as a linear system for which iterative methods may be applied, with convergence to the exact solution when it exists.[6] Filtered backprojection algorithms, by comparison, may cause unwanted smoothing of fine features. However, iterative solutions of large linear systems have greater computational complexity. For image size $N = 1024$, the execution time was on the order of 10–100 s on a small laptop computer (single core, using Matlab). The number of required iterations depends on the data and applications. There are several ways to speed up the algorithm, e.g., by using only a single quadrant transform (each operator $\mathcal{R}^i$ in Eqn. 9 is injective[6]), or by processing the image in disjoint blocks. For block size $N \leq 64$, if not larger, the matrix representation of the inverse operator $(\mathcal{B} \circ \mathcal{R})^{-1}$ [or, alternatively, $(\mathcal{R}^+ \circ \mathcal{R})^{-1}$] may be precomputed to arbitrary accuracy, and inversion carried out by matrix multiplication. The DRT algorithm also seems well suited for parallelization.

While the example data presented in Sec. 3 were obtained with the now inoperative Envisat satellite, scalloping is still a concern for existing SAR systems. Even the Terrain Observation by Progressive Scans (TOPS) imaging mode, whose design promises to eliminate the azimuth dependence problem, may exhibit some scalloping caused by electronic beam steering.[16] Since scalloping is periodic with a fixed orientation, frequency (Fourier) domain filtering is a natural choice for descalloping algorithms. As shown in Ref. 3, however, spectral modifications require much care to avoid secondary artifacts. The main strength of the composite-transform method is the ease of implementing a filter in the DRT domain. It should also work well for non-periodic noise, e.g., stripe noise caused by detector-to-detector variations in optical pushbroom-type systems. Finally, we note that it should be possible to combine the rotation-invariant invertible edge operator $\mathcal{L}$ with other operators, such as generalized Radon transforms that integrate functions on other shapes than lines.

REFERENCES

[1] Hawkins, R. K. and Vachon, P. W., "Modelling SAR scalloping in burst mode products from RADARSAT-1 and ENVISAT," in [*Proc. of CEOS Working Group on Calibration/Validation - SAR Workshop*], ESA Pub. SP-526, London, UK (Sep. 2002).

[2] Bamler, R., "Optimum look weighting for burst-mode and ScanSAR processing," *IEEE Trans. Geosci. Remote Sens.* **33**, 722–725 (May 1995).

[3] Romeiser, R., Horstmann, J., Caruso, M. J., and Graber, H. C., "A descalloping postprocessor for ScanSAR images of ocean scenes," *IEEE Trans. Geosci. Remote Sens.* **51**, 3259–3272 (Jun. 2013).

[4] Ripel, Ø., *Kompensasjon av scallop og gain-shift i oljesøldeteksjon (Compensation for scalloping and gain shift in oil spill detection)*, Master's thesis, University of Oslo, Department of informatics (May 2008). In Norwegian.

[5] Schiavulli, D., Sorrentino, A., and Migliaccio, M., "An innovative technique for postprocessing descalloping," *IEEE Geosci. Remote Sens. Lett.* **10**, 424–427 (May 2013).

[6] Landmark, K., Solberg, A. H. S., Albregtsen, F., Austeng, A., and Hansen, R. E., "A Radon-transform-based image noise filter - with applications to multibeam bathymetry," *IEEE Trans. Geosci. Remote Sens* . To appear; published online 15 June 2015.

[7] Einsiedler, M. and Ward, T., [*Functional Analysis, Spectral Theory, and Applications*] (Mar. 2015). Draft version.

[8] Jähne, B., [*Digital Image Processing*], Springer, Berlin Heidelberg New York, 6th revised and extended ed. (2005).

[9] Natterer, F. and Wübbeling, F., [*Mathematical Methods in Image Reconstruction*], Soc. Ind. Appl. Math., Philadephia, PA/US (2001).

[10] Götz, W. A. and Druckmüller, H. J., "A fast digital Radon transform—an efficient means for evaluating the Hough transform," *Pattern Recognition* **29**(4), 711–718 (1996).

[11] Brady, M. L., "A fast discrete approximation algorithm for the Radon transform," *SIAM J. Comput.* **27**(1), 107–119 (1998).

[12] Press, W. H., "Discrete Radon transform has an exact, fast inverse and generalizes to operations other than sums along lines," *Proc. Natl. Acad. Sci. USA (PNAS)* **103**(51), 19249–19254 (2006).

[13] Saad, Y. and Schultz, M. H., "GMRES: A generalized minimal residual algorithm for solving nonsymmetric linear systems," *SIAM. J. Sci. Stat. Comput.* **7**, 856–869 (July 1986).

[14] Solberg, A. H. S., "Remote sensing of ocean oil-spill pollution," *Proceedings of the IEEE* **100**, 2931–2945 (Oct. 2012).

[15] Solberg, A. H. S., Brekke, C., and Husøy, P. O., "Oil spill detection in Radarsat and Envisat SAR images," *IEEE Trans. Geosci. Remote Sens.* **45**, 746–755 (Mar. 2007).

[16] Wollstadt, S., Prats, P., Bachmann, M., Mittermayer, J., and Scheiber, R., "Scalloping correction in TOPS imaging mode SAR data," *IEEE Trans. Geosci. Remote Sens.* **9**(4), 614–618 (2012).